INFLUENCE OF THE IMPURITIES TO THE COMPOSITE MATERIALS IN LASER ABLATION PHENOMENA

Alexandru COCEAN[1], Iuliana COCEAN[2] and Silviu GURLU[3]

Study of physico – chemical phenomena and processes that may occur during laser ablation, plasma plume expansion from target to support and finally deposition on special supports was performed on a nonhomogeneous target. The target is made of silver with impurities of iron and nickel. Experimental study was assisted and completed by COMSOL simulations. The thin films were deposited on different supports using Pulsed Laser Deposition (PLD) method. The aim was to investigate the physico-chemical characteristics of the obtained thin films, searching for the influence of parameters and conditions on the quality of the layer and for a better understanding of the mechanisms that induce the observed phenomena. Considering the possibility of using silver films as applications in the production of laser mirrors, laser damage threshold and damage magnitude at different fluences are experimentally and by means of COMSOL investigated and a very good similitude is obtained between the experimental and numerical results.

Keywords: PLD, COMSOL, fluids instabilities, nonhomogeneous target, composite materials

1. Introduction

Silver layer produced by pulsed laser deposition method (PLD) aimed for laser mirrors require specific properties (i.e. damage threshold) and the study with respect to those is presented in this paper. [1]. Laser ablation plasma behavior during pulsed laser deposition has been extensively studied by means of various experimental and simulation techniques. [1, 3 - 14]. Therefore, droplets formation on the deposited layers that can seriously damage both the quality of the deposited thin layer and the morphology [15] is treated herein from the perspective of Plateau-Rayleigh, Rayleigh – Taylor and Richtmyer – Meshkov instabilities, as well as crown splash, based on the numerical study of co-existing phases in the ablated material correlated with experimentally observed morphology (SEM, AFM) and measured, composition, dynamic, structure (EDX, FTIR, XRD, ICCD camera). Previous papers expand Plateau – Rayleigh instability (PRI) theory from liquids and thermocapillary suppression [16 - 18] and solid–liquid interface [19]

[1] Alexandru Ioan Cuza University of Iasi, Faculty of Physics, 11 Carol I Bld., Iasi, Romania
[2] lexandru Ioan Cuza University of Iasi, Faculty of Physics, 11 Carol I Bld., Iasi, Romania
[3]Alexandru Ioan Cuza University of Iasi, Faculty of Physics, 11 Carol I Bld., Iasi, Romania e-mail: sgurlui@uaic.ro

to dielectric elastomer films [20], in solids as simple phase separation [21], during reorganization of silicon macro pores process [22] and usage for preparation of the nanoparticles in photonics applications [23]. The other fluid break – up phenomenon to consider is the Rayleigh – Taylor instability (RTI) that occurs at the interface of two fluids of different densities when the lighter liquid pushes the heavier one under gravity or other forces such as those generated by explosions [24 - 26]. This instability is used to explain mushroom clouds in volcanic eruptions, nuclear and supernova explosions. RTI was also studied at "large and small scale" as to the bubbles internal structure and cascade wavelengths [27]. Richtmyer – Meshkov instability (RMI) regarding shock – wave that occurs when two fluids of different densities are impulsively accelerated [28, 29] and "crown splash" [17, 30] are the next phenomena related to fluids break – up that will be addressed in this work. With this paper, it is first time to considering the three instabilities - PRI, RTI, RMI – and crown splash for droplets formation during laser ablation and deposition and they are discussed based on experiments and COMSOL simulation of co-existing ablation phases. This paper will present the techniques of pulsed laser deposition (PLD) used as a new method to produce thin layers of silver citrate. The three directions of study – droplets formation during PLD, laser damage threshold of the deposited layer and silver citrate produced with PLD technic are all connected by the same numerical simulation in COMSOL, same target and the phenomena and processes observed are interconnected for all the three findings presented with this paper.

2. Materials and methods

The experiments were carried out on the installation for PLD (pulse laser deposition) and LIBS (laser induced breakdown spectroscopy) from Atmosphere Optics, Spectroscopy and Lasers Laboratory described in reference [1, 2, 6] using a target mainly consisting of silver, containing also iron and nickel impurities.
The target was produced by thermal, mechanical and chemical processes from silver jewelry that had been previously doped with nickel and iron. Sodium tetra - borate ($Na_2B4O_7 \cdot 10H_2O$) and sodium borohydride ($NaBH_4$) have been used during these procedures for cleaning – up the oxides from the target by conversion of silver cations to atomic state [31, 32]. The other metals in the target composition (iron and nickel) have also been converted from their ionic state in oxides and hydroxides into atoms during the mentioned chemical treatment. The silver target was further cleaned up with sodium bicarbonate (as catalyst) in presence of aluminum foil (which has sulfur higher chemical affinity) to extract the eventual sulfur that might had been acquired by the target when in contact with the atmosphere and when resulted silver sulfide (Ag_2S). The silver target has been ablated using a YG 981E/IR-10 laser system, and the parameters: τ=10 ns

pulse width, λ=532 nm wavelength, α=45° incident angle and ν = 10 Hz pulse repetition time (Figure 1). The pressure in the deposition chamber was $3 \cdot 10^{-2}$ Torr. For a better understanding of the processes and phenomena that take place in the pulsed laser ablation and deposition of thin films using a target made of silver and containing impurities of iron and nickel, ablation simulation in COMSOL Multiphysics. Under the study presented in this work, two simulations were performed: for laser heating of the target including thermal effects in the vacuum chamber atmosphere and a second one for laser heating of the silver thin film to evaluate laser damage threshold and damage magnitude under different fluences. As shown in previous publications [1, 2, 33], Heat Transfer in Solids is the most appropriate COMSOL module to describe the ablation as a heating effect of laser irradiation interaction with the target, generating the phase change into liquid, gas and plasma states.

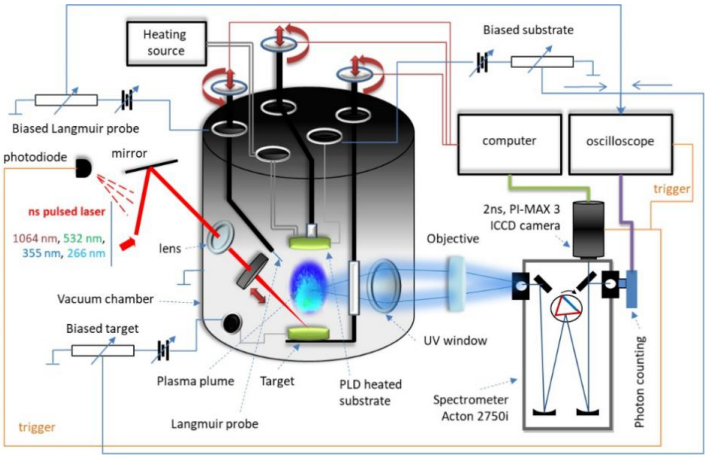

Fig. 1. Experimental set-up.

3. Results and discussions

Study of fluid phase influence on thin film morphology

The new model that we introduced in COMSOL for this study calculates and acquires data for the heat effects from both target surface and volume and in the deposition chamber environment designed in convenient geometry to best cover all the areas of interest. Though the previous models [1, 2] take into consideration the heat loss in the surrounding environment, they do not allow data acquisition on the thermal effects due to heat diffusion in the surrounding environment, because of the geometry and the mesh. The results in element finite method – as the case for COMSOL too – are nodal solutions based on the discretization of a geometrical structure. Thus, if the previous models are applicable when there is an

interest only for the heating effects on the target and in the target volume, this new model provides also information on the temperature developed under heat diffusion in a certain volume of interest (geometrically designed) from the surrounding atmosphere. The inconvenient for such complex model consists in the much longer time needed to process the simulation and the model should be used only when there is a good reason, in order to optimize the work. Because in this study there is an interest for the material phase states (reveled by the material temperatures) during its travel from the target to support, the extended model presented herein has the role to complete such information and, therefore, its use is justified. For such purpose, the geometry consists in two rectangular prisms, one of them representing the environmental atmosphere in the deposition chamber on the direction of the target, and a second one virtually representing the silver target covered by a silver layer containing iron and nickel impurities (Figure 2).

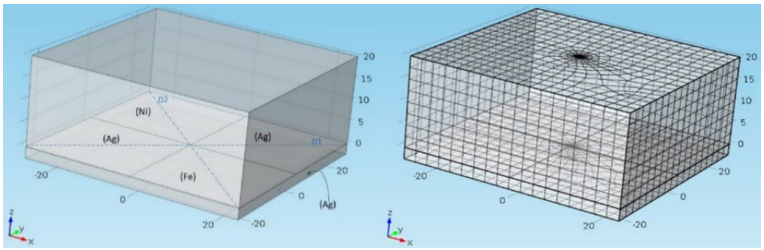

Fig. 2. Geometry with materials and mesh for COMSOL simulation

Once the material selected from COMSOL library, all its parameters and constants are automatically provided. COMSOL provides polynomial functions on ranges of temperatures only up to the temperature near melting point for density (873^0C for Ag, 960^0C for Fe, 1728^0C for Ni). Polynomial equations for the specific heat at constant pressure and for the thermal conductivity are provided by COMSOL library up to the melting point of each material (1235^0C for Ag, 1810^0C for Fe, 1728^0C for Ni). For higher temperatures, the "nearest function" was chosen as extrapolation option for each of them. Refractive indexes and extinction coefficients of each of the materials at initial temperature T= 293.15 K (only one pulse is simulated) and laser beam wavelength λ = 532 nm were introduced as it follows: $n_{Ag} = 0.054007$; $k_{Ag} = 3.4290$; $n_{Fe} = 2.8954$; $k_{Fe} = 2.9179$; $n_{Ni} = 1.8775$; $k_{Ni} = 3.4946$ [34]. Laser standard deviations along x – coordinate and along y – coordinate $\sigma x = \sigma y = 168$ μm, laser spot center coordinates, pulse width of 10 ns and laser energies of 100 mJ, 150 mJ and and 180 mJ were introduced in accordance with experiment. Important preliminary, quick information about heating effects on the target and in its surrounding environment in the deposition chamber are provided by 3D and 2D plots generated either as 3D isosurface plots pre-set in COMSOL or as 2D plots generated based on 3D cut

plans defined by the coordinates appropriate to the area of interest for highlighting the useful data (Figure 3 and 4). In the 3D plot of isosurface contours (Figure 4) temperature was set to a minimum of 10^5 K order for obtaining information about the magnitude in volume of the heating conditions that favor the plasma formation on the target and heat transfer in the surrounding environment that allows plasma state conditions at pulse width of 10 ns, for a laser energy of 150 mJ.

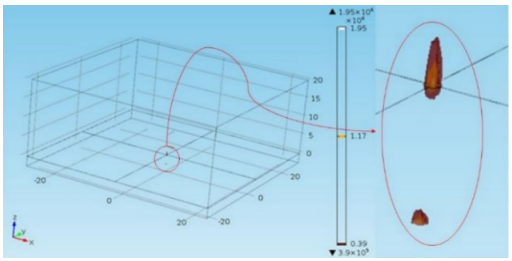

Fig. 3. 3D Plot representing the Isosurface where heating is high enough to favor the plasma formation on the target and heat transfer in the surrounding environment

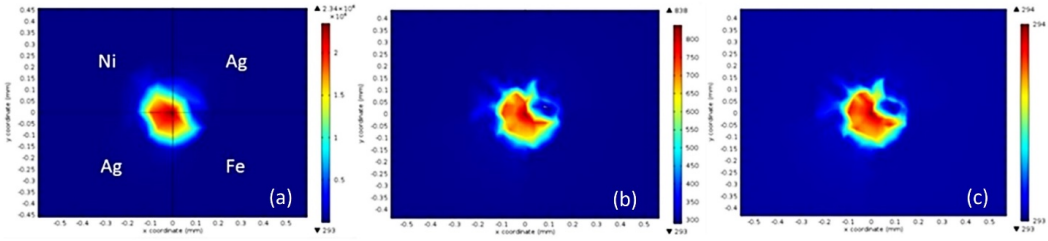

Figure 4. 2D Heating plots in xOy plane at 10 ns when using 150 mJ laser energy: a) on the target surface; b) at 10 mm height from target; c) at 20 mm height from target

It is evidenced an important amount of plasma phase formation confirmed also by the 1D plots in Figures 5 and the diagrams in Figures 6. The environmental heating considers only the heat transfer from the target to the environment and does not consider the heat transfer between the ablation plume and the environment when the plume crosses it. However, that would add more heating in the deposition chamber, the environment temperature conditions on the ablated plume direction of movement being even more favorable to preserve the plasma state of the ablated material. The 2D plots at 10 ns for 150 mJ laser energy, generated based on xOy cut planes on target surface and on planes placed at different distances (z) from the target surface (Figure 4: b) z = 10 mm and c) z = 20 mm) provide the information about target surface heating due to laser irradiation and heat diffusion and thermal effect in the environment from the deposition chamber. The simulation shows conditions favorable for melted phase up to 10 mm distance from the target in the deposition chamber environment

(Figure 7). This information is important to estimate thermal conditions developed in the deposition chamber for a phase state evaluation of the ablated material. The thermal effect is calculated at different energies, i.e. 100 mJ, 150 mJ and 180 mJ – same as in the experimental study - and for that purpose, a parametric sweep of 100 mJ, 150 mJ and 180 mJ is used in the simulation. 1D plots, based on *3D Cut Lines* across diagonal D_1 and diagonal D_2 (Figure 3), have been generated as phase change diagrams T(d) (Figure 5).

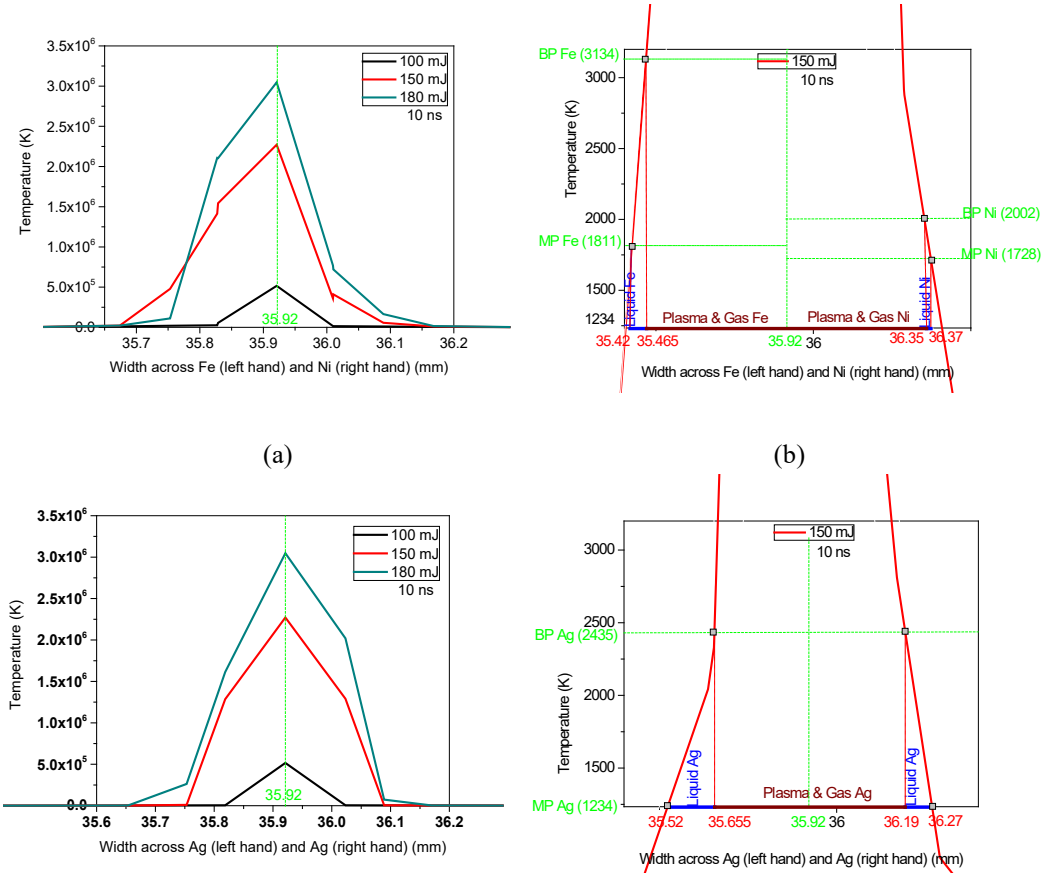

Fig. 5. Phase change diagrams T(d) on the target irradiated surface after 10 ns for: iron and nickel at different energies (a) and their co-existing phases at 150 mJ (b); silver at different energies (c) and its co-existing phases at 150 mJ (d)

The phase change is established in COMSOL based on the temperatures achieved compared to the melting and boiling points of the materials. Conditions of ablation at 10 ns (pulse width) after laser ignition are met on an average area of 0.468 mm^2 for 100 mJ laser beam energy, 0.577 mm^2 for 150 mJ and 0.617 mm^2 for 180 mJ, calculated based on the phase diagrams in Figure 5 and considering

that ablation includes melted material, gas and plasma. Based on the diagrams in Figure 5, ratio phases at 10 ns after laser ignition is studied for each of the laser energy used to irradiate the target (Figure 6). The following observation is to be noticed: silver from all the three elements in the target is with the most potential to generate liquid phase, followed by iron and nickel ("Phase rate per element" Figure 6).

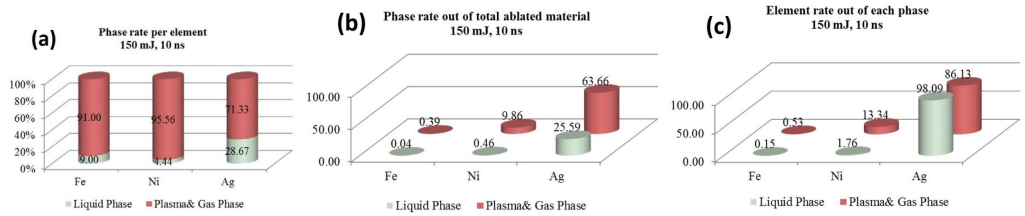

Fig. 6. Study of phases fractions during ablation, for t = τ = 10 ns, based on COMSOL simulation. (a) Phase rate per element developed during laser ablation at 150 mJ on COMSOL simulation; (b) Phase rate out of total ablated material based on COMSOL simulation; (c) Element rate out of each phase during ablation to different energies based on COMSOL simulation.

In Fig. 6 the calculation was made based on the results obtained in COMSOL simulation: d_{liq}[mm] is the size of the liquid phase developed for each element on the irradiated spot diagonal; d_{gas}[mm] is the size of the gas &plasma phase developed for each element on the irradiated spot diagonal; d_{abl}[mm] is the total ablated size on the irradiated spot diagonal for each element. The phase rates (Figure 6 a) were calculated as it follows: $\%liq_{sim}$ represents the percentage of liquid phase resulted out of total ablated phase of each element (liquid + gas & plasma) based on the simulation; $\%gas_{sim}$ represents the percentage of gas & plasma phase resulted out of total ablated phase of each element (liquid + gas & plasma) based on the simulation for each element. Phase rate out of total ablated material (Fig. 6 b) is the phase rate corrected based on the initial elemental composition of the target using the following formulae, where %EDS is the target initial elemental composition $\%liq_{abl}$ represents the percentage of liquid phase of each component (element); $\%gas_{abl}$ represents the percentage of gas & plasma phase of each component (element)**.** The element rate (%Me) out of each phase (liq_{tot} and gas_{tot}), in Figure 6c, was calculated as it follows: $\%Me/liq_{tot}=(\%liq_{abl}/Total_{liq})*100$ represents the percentage of each element component out of the total liquid phase; $\%Me/gas_{tot}=(\%gas_{abl}/Total_{gas})*100$ represents the percentage of each element component out of the total liquid phase. Based on the target elemental composition analyzed in EDX, as silver is the majoritarian component (89.25%), the most contributing to the ablated liquid phase is the silver liquid state (97.15% for laser beam energy of 100 mJ, 98.09% for 150 mJ, and 98.46% for 180 mJ), as Figure 7 shows. Also, from the total ablated material in liquid and gas/plasma state, silver liquid state represents

around a quarter (28.15% when target irradiated with 100 mJ laser beam energy, 25.59% for 150 mJ, and 23.24% for 180 mJ laser beam energy), as it states in Fig. 6. The thermal effects resulted in the simulation reflect the influence of nonhomogeneous composition of the irradiated material. In addition to the optical properties of each component (absorbance, reflectivity, heat capacity, etc.) that influence laser heating and heat diffusion, other effects and processes occur, such as thermal equilibrium at contact regions of the components where heat exchange takes place [2]. The phases of each element resulted during target ablation under laser irradiation are the sources for the film that will be accumulated on the support and they will be influenced by the temperature in the atmosphere from the deposition chamber. As noticed in the preliminary observation regarding thermal effects in the surrounding environment of the target (3D plots and 2D plots from Fig. 3 and Fig. 4, respectively), significant heating is noticed in the target neighborhoods due to the heat diffusion. For a better evaluation of the thermal effects in the deposition chamber atmosphere, 1D plots of temperature variation with the distance from the target, are generated (Fig. 7).

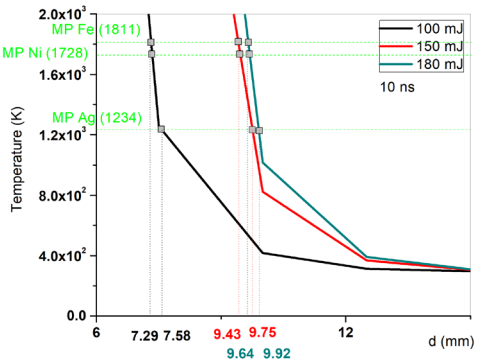

Fig. 7. Thermal effects in the deposition chamber target surrounding atmosphere in (x, y, z) = (0, 0, z) and z Є [0, d] and d=20 mm (distance between target and support)

The nodes to collect results were appointed as (x, y, z) = (0, 0, z), meaning that x and y are set in the spot center and z is along the vector normal on the target surface pointing to the support surface. The range for z is set as per experimental set-up of the target and support, z Є [0, d] where d is the distance between target and support and d = 20 mm. The step time to acquire data is τ/25, but only the plots at 10 ns and 20 ns after laser ignition are presented herein to observe the thermal effect due to pulsed laser irradiation (10 ns, the pulse width), and the thermal effect due to heat diffusion (20 ns after laser ignition, when the heat sourced by laser power dissipates into the volume of surrounding media). The simulation provides information about fluid phase developed during ablation and deposition. Fluids are susceptible to enter into instabilities generated under

different perturbing phenomena leading to break-ups into their flowing mass. Droplets noticed in SEM images on the deposited films, but also on the target are the evidence that PRI, RTI and RMI have been developed during ablation and plasma plume movement from target to the deposition support. Splash crown effect is also noticed on the SEM images (Figure 8 a-d) of the thin layers obtain at the higher energy (180 mJ) as ring shaped droplets compared to the pearl shaped droplets obtained at lower energy (100 mJ). These instabilities are based on the induced perturbing phenomena such as electromagnetic field of laser beam for the first 10 ns, the electric field of the diffusion current generated by the charged carriers (ions in plasma) during their motion and the phase states developed during ablation and evidenced in the numerical simulation in COMSOL

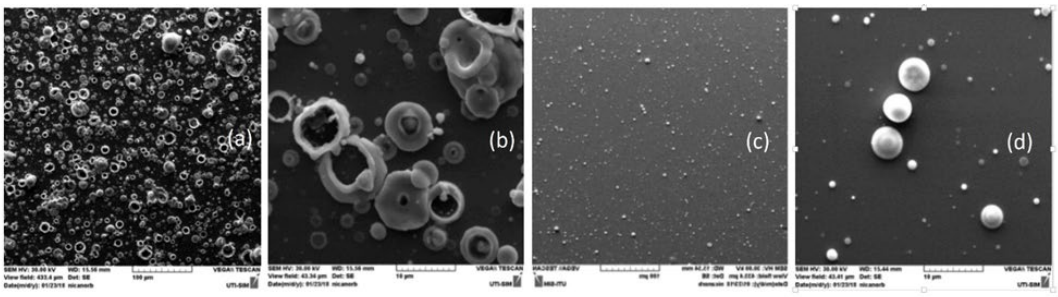

Figure 8. Compared SEM images of droplets on the thin films A (180 mJ) and B (100 mJ): (a) Sample A (180 mJ) 500x; (b) Sample A (180 mJ) 5kx; (c) Sample B (100 mJ) 500x; (d) Sample B (100 mJ) 5kx

Study of damage threshold and damage magnitude

A second simulation in COMSOL was conducted for this study to compare numerical results with SEM analysis in order to determine either damage threshold and damage magnitude can be numerically anticipated. The simulation corresponds to laser irradiation of the experimentally produced and analyzed sample C. Laser parameters are the same as for the experimental study of damage threshold, using a parametric sweep for energies. For the purpose of simulation, the *Heat Transfer in Solids* module and equations as per Cocean et al, 2017 [1, 2] were used to model the heat source, as presented before. The aim of the study being to determine the heating of the target, the model is set this time only for the target with the corresponding geometry and mesh [1]. Geometry was set up consisting of a cylinder (disc) covered by a layer. EDX analysis of the film deposited showed that its content in silver is almost 100%. For that reason, the material added to the geometry is only silver. The silver layer of 240 nm is virtually deposited on a glass slab of 50.8 mm diameter and 20 mm thickness. The melting point is considered the starting temperature when the ablation conditions are met. In order to quantify the computed damage magnitude, the distance on abscise (corresponding to the distance on the diagonal in Figures 9 a-b) is

measured for temperature higher than melting point of Silver (1239 K). Also, the results of the simulation show that melting condition is not met on the back side of the layer (Fig. 9 b) at any of the fluences used in experiment and that means no damage goes through all the layer thickness.

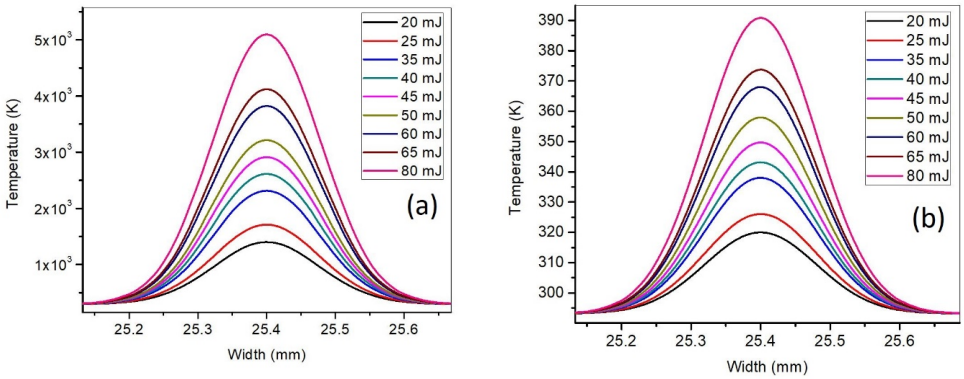

Figure 9. COMSOL results of layer heating under pulsed laser irradiation: (a) phase change temperature conditions on laser irradiated surface at different laser irradiation energies; (b) thermal effects on layer back side surface under laser irradiation at different energies

Table 1

Experimental versus simulated results

Energy (mJ)	Density of energy (J/cm2)	Threshold radius size (μm) Experimental (SEM)	Threshold radius size (μm) COMSOL
20 mJ	45.11	-	-
25 mJ	56.39	138.42 μm	140 μm
35 mJ	78.95	195.44 μm	191 μm
40 mJ	90.22	210.56 μm	209 μm
45 mJ	101.50	216.08 μm	223 μm
65 mJ	146.61	266.48 μm	263 μm
80 mJ	180.45	287.72 μm	283 μm

The threshold represents in this case the pulsed laser fluence or density of energy in J/cm^{2}that induces damages on the thin layer. The threshold, magnitude of measured and simulated damages are compared and listed in Table 1. For the threshold, the standardized area was used and that is calculated with the formula $A=0.5\pi r^2$ where r =168 μm is the laser spot radius [1, 2, 35]. Threshold starts right after 45.11 J/cm^2 density of energy. Magnitude of damages evolution with density of energy would be the fitting exponential line The experimental size of the damages on the thin layer resulted under pulsed laser irradiation were measured on the SEM images (Figure 10).

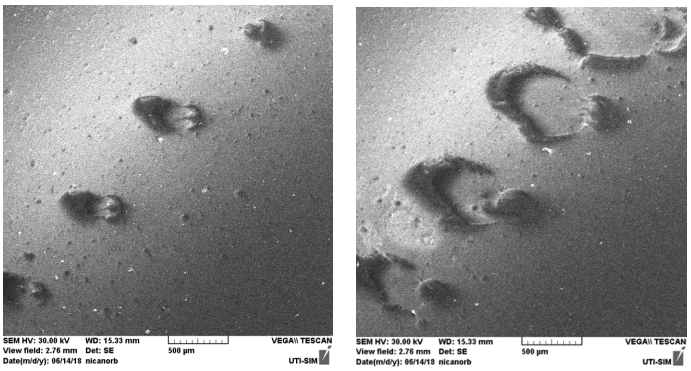

Figure 10. SEM images of the laser irradiated damaged areas on the Silver layer surface

4. Conclusions

The study on the nonhomogeneous target consisting of silver with impurities of iron and nickel under pulsed laser irradiation during PLD method provided important information as to the composition and morphology of the resulted thin layer and to the plasma plume of ablation. Fluid break – up due to the Plateau – Rayleigh, Rayleigh – Taylor and Richtmyer – Meshkov instabilities have been observed due to their effects in droplets and crown splash formation.. Understanding the instabilities that occur at interfaces of the fluid states generated during ablation and plasma plume motion from target to the support are important for a better set up of parameters and conditions of work to achieve the desired results for the pulsed laser deposited thin films. COMSOL simulations assisting the experimental work conducted for the study presented herein provide supplementary information for a better understanding of the phenomena that occur during ablation and deposition under pulsed laser irradiation applied to a nonhomogeneous target. The numerical model developed in COMSOL to simulate laser heating in our previous published work [1, 2] has been further extended in order to acquire numerical results for environmental space surrounding the target in the deposition chamber. The extended numerical model presented herein requires a very long time to process the data and it is recommended only when environmental heating is relevant for the study. Otherwise, the initial model is the recommended when only heat effects on the target are to be studied. Damage threshold and damage magnitude induced by laser irradiation in the deposited layer is also studied and the results are found to be similar in both experimentally work and simulation in COMSOL, making the numerical model developed in COMSOL reliable for such preliminary estimation of laser damage threshold.

Acknowledgments

This research was funded by Ministry of Research, Innovation and Digitization, project FAIR_09/24.11.2020 and by the Executive Agency for Higher Education, Research, Development and Innovation, UEFISCDI, ROBIM-project number PN-III-P4-ID-PCE2020-0332

REFERENCES

[1] *A. Cocean, I. Cocean, S. Gurlui, F. Iacomi*, Study of the pulsed laser deposition phenomena by means of Comsol Multiphysics, U.P.B. Sci. Bull., Series A, Vol. 79, Iss. 2, 2017

[2] *A. Cocean, V. Pelin, M. M. Cazacu, I. Cocean, I. Sandu, S. Gurlui, F. Iacomi*, Thermal Effects Induced By Laser Ablation In Non-Homogeneous Limestone Covered By An Impurity Layer, Applied Surface Science Volume 424, Part 3, 1 December 2017, Pages 324-329

[3] *M. Stafe, I. Vladoiu, C. Negutu, I.M. Popescu*, Experimental investigation of the nanosecond laser ablation rate of aluminum, Rom. Rep. Phys. 60(3) (2008) 789-796.

[4] *S. Gurlui, M. Sanduloviciu, M. Strat, G. Strat, C. Mihesan, M. Ziskind, C. Focsa*, Dynamic space charge structures in high fluence laser abl. plumes, J. Optoelectron. Adv. M. 8(1) (2006) 148

[5] *S. Gurlui, M. Agop, P. Nica, M. Ziskind, C. Focsa*, Experimental and theoretical investigations of a laser produced aluminum plasma, Phys. Rev. E 78(2) (2008) 026405 part 2.

[6] *I. Cocean, A. Cocean, C. Postolachi, V. Pohoata, N. Cimpoesu, G. Bulai, F. Iacomi, S. Gurlui*, Alpha keratin amino acids behvior under high fluence laser interaction. Medical applications, Applied Surface Science 2019, DOI: 10.1016/j.apsusc.2019.05.207

[7] *B. Le Drogoff, J. Margot, M. Chaker et al.,* "Temporal characterization of femtosecond laser pulses induced plasma for spectrochemical analysis of aluminumalloys," Spectrochimica Acta Part B, vol. 56, no. 6, pp. 987–1002, 2001

[8] *C. Hernandez, H. Roche, C. Pocheau, C. Grisolia, L. Gargiulo, A. Semerok, A. Vatry, P. Delaporte, L. Mercadier*, Development of a Laser Ablation System Kit (LASK) for Tokamak in vessel tritium and dust inventory control, Fusion Engineering and Design, Volume 84, Issues 2–6, Pages 939–942, June 2009

[9] *N. Bekrisa, J.P. Coadb, C. Grisoliac, J. Likonend, A. Semeroke, K. Dylstf, A. Widdowsonb*, Fusion Technology related studies at JET: Post-mortem tile analysis with MKII-HD geometry, In situ laser detritiation and Molecular Sieve Bed detritiation, Journal of Nuclear Materials, Volume 417, Issues 1–3, Pages 1356–1360, 1 October 2011

[10] *C. Grisolia, A. Semerok, J.M. Weulersse, F. Le Guern, S. Fomichev, F. Brygo, P. Fichet, P.Y. Thro, P. Coad, N. Bekris, M. Stamp, S. Rosanvallon, G. Piazza*, In-situ tokamak laser applications for detritiation and co-deposited layers studies, Journal of Nuclear Materials, Volumes 363–365, , Pages 1138–1147, 15 June 2007

[11] *L. Mercadier, J. Hermann, C. Grisolia, A. Semerok*, Analysis of deposited layers on plasma facing components by laser-induced breakdown spectroscopy: Towards ITER tritium inventory diagnostics, Journal of Nuclear Materials, Volume 415, Issue 1, Supplement, Pages S1187–S1190, 1 August 2011

[12] *R. Fantoni, S. Almaviva, L. Caneve, F. Colao, A. M. Popov, G. Maddaluno*, Development of Calibration-Free Laser-Induced-Breakdown-Spectroscopy based techniques for

deposited layers diagnostics on ITER-like tiles, Spectrochimica Acta Part B: Atomic Spectroscopy, Volume 87, Pages 153–160, 1 September 2013

[13] *S. Gurlui, G. O. Pompilian, P. Nemec, V. Nazabal, M. Ziskind, C. Focsa,* Plasma Diagnostics in Pulsed Laser Deposition of GaLaS Chalcogenides, Appl. Surf. Science, 278, Pages 352-356 (2013)

[14] *S. Gurlui, C. Focsa,* Plasma Science, Laser Ablation Transient Plasma Structures Expansion in Vacuum, IEEE Transactions on Volume: PP, Issue: 99, DOI: 10.1109/TPS.2011.2151884, Publication Year: (2011).

[15] *J. P. Singh and S. N. Thakur*, "Laser-Induced Breakdown Spectroscopy," Elsevier Science, Amsterdam, 2007

[16] *B. Vajdi Hokmaba, S. Faraji, T. Ghaznavi Dizajyekan, B. Sadri and E. Esmaeilzadeh*, Electric field-assisted manipulation of liquid jet and emanated droplets, Inernational Journal of Multi phase Flow, DOI: 10.1016/j.ijmultiphaseflow.2014.03.009, 31 March 2014

[17] *Eduardo Castillo-Orozco, Ashkan Davanlou, Pretam K. Choudhury, Ranganathan Kumar*, Droplet impact on deep liquid pools: Rayleigh jet to formation of secondary droplets, PHYSICAL REVIEW E 92, 053022 (2015), DOI: 10.1103/PhysRevE.92.053022

[18] *Y. - J. Chen, R. Abbaschian and P. H. Steen*, Thermocapillary suppression of the Plateau–Rayleigh instability: a model for long encapsulated liquid zones, J. Fluid Mech. (2003), vol. 485, pp. 97–113. c 2003 Cambridge University Press DOI: 10.1017/S0022112003004373

[19] *Sabrina Haefner, Michael Benzaquen, Oliver Baumchen, Thomas Salez, Robert Peters, Joshua D. McGraw, Karin Jacobs, Elie Raphae & Kari Dalnoki-Veress*, Influence of slip on the Plateau–Rayleigh instability on a fibre, 2015, NATURE COMMUNICATIONS | 6:7409 | DOI: 10.1038/ncomms8409 |www.nature.com/naturecommunications

[20] *Saman Seifi and Harold S Park*, Electro-elastocapillary Rayleigh-Plateau Instability in Dielectric Elastomer Films, DOI: 10.1039/C7SM00917H , Soft Matter 13(23), May 2017

[21] *Chen Xuan and John Biggins*, Plateau-Rayleigh instability in solids is a simple phase separation, Phys. Rev. E 95, 053106, 11 May 2017

[22] *M. Garín, C. Jin, D. Cardador, T. Trifonov, R. Alcubilla*, Controlling Plateau-Rayleigh instabilities during the reorganization of silicon macropores in the Silicon Millefeuille process, Scientific Reports volume 7, Article number: 7233 (2017), Dan-Dan Liu, Yu-mei Xu, Xian-ting Ding, Jian Yang, and Zhi-jun Ma, Utilizing the Plateau-Rayleigh Instability with Heat-Driven Nano-Biosensing Systems, Journal of Laboratory Automation 2015, Vol. 20(4) 463–470, DOI: 10.1177/2211068215575688

[23] *H.J. Kull*, Theory of the rayleigh-taylor instability, PHYSICS REPORTS (Review Section of Physics Letters) 206, No. 5 (1991) 197-325. North-Holland

[24] *A. R. Piriz, O. D. Cortázar, J. J. López Cela, N. A. Tahir,* The Rayleigh-Taylor instability, Am. J. Phys. 74 12, December 2006, DOI: 10.1119/1.2358158

[25] *Sharp, D.H.* (1984). "An Overview of Rayleigh-Taylor Instability". Physica D. 12 (1): 3–18. Bibcode:1984 doi:10.1016/0167-2789(84)90510-4

[26] *Schneider, M., Dimonte, G. & Remington, B.* 1998 Large and small scale structure in rayleigh-taylor mixing. Phys. Rev. Lett. 80, 3507–3510.

[27] *Richtmyer, R.* 1960 Commun. Pure & Appl. Math. 13, 297.

[28] *S. I. Abarzhi and M. Herrmann*, New type of the interface evolution in the Richtmyer-Meshkov instability, Center for Turbulence Research Annual Research Briefs 2003

[29] *Li V. Zhang, Philippe Brunet, Jens Eggers, and Robert D. Deegan*, Wavelength selection in the crown splash, PHYSICS OF FLUIDS 22, 122105, 19 November 2010, doi:10.1063/1.3526743

[30] *M. M. Cook and J. A. Lander*, Use of Sodium Borohydride to Control Heavy Metal Discharge in the Photographic Industry, Journal of Applied Photographic Engineering 5 144-147 (1979)

[31] *Cotton, F. Albert; Wilkinson, Geoffrey* (1966). Advanced Inorganic Chemistry (4th Ed.). New York:Interscience, 1980
[32] *G. Poulain, D. Blanc, A. Kaminski, B. Semmache, M. Lemiti,* Modeling of Laser Processing for Advanced Silicon Solar Cells, COMSOL Conference 2010 Paris.
[33] Resource web: https://refractiveindex.info/
[34] ISO 21254-2:2011 and ISO 21254-3:2011